

Title	Influence of Humidity on Layer-by-Layer Growth and Structure in Coordination Networks
Author(s)	Aoki, Kentaro; Matsuzawa, Toshitaka; Suetsugu, Kota; Hara, Mitsuo; Nagano, Shusaku; Nagao, Yuki
Citation	Inorganic Chemistry, 63(15): 6674-6682
Issue Date	2024-04-01
Type	Journal Article
Text version	author
URL	http://hdl.handle.net/10119/19947
Rights	Kentaro Aoki, Toshitaka Matsuzawa, Kota Suetsugu, Mitsuo Hara, Shusaku Nagano, Yuki Nagao, Inorganic Chemistry, 2024,63, 15, 6674–6682. This document is the Accepted Manuscript version of a Published Work that appeared in final form in Inorganic Chemistry, copyright (c) American Chemical Society after peer review and technical editing by the publisher. To access the final edited and published work see https://doi.org/10.1021/acs.inorgchem.3c04526 .
Description	

Influence of Humidity on Layer-by-Layer Growth and Structure in Coordination Networks

Kentaro Aoki[†], Toshitaka Matsuzawa[†], Kota Suetsugu[‡], Mitsuo Hara[‡], Shusaku Nagano[§], Yuki Nagao^{†*}

[†] School of Materials Science, Japan Advanced Institute of Science and Technology, 1-1 Asahidai, Nomi, Ishikawa, 923-1292, Japan

[‡] Department of Molecular and Macromolecular Chemistry, Graduate School of Engineering, Nagoya University, Furo-cho, Chikusa, Nagoya 464-8603, Japan

[§] Department of Chemistry, College of Science, Rikkyo University, 3-34-1 Nishi-Ikebukuro, Toshima, Tokyo, 171-8501, Japan

Abstract

Metal–organic frameworks (MOFs) are promising materials because of their high designability of pores and functionalities. Especially, MOF thin films and their properties have been investigated toward the application in nanodevices. Typically, MOF thin films are fabricated using a bottom-up method such as layer-by-layer (LbL) growth in air. Because the water molecules can coordinate and replace with organic linkers during synthesis, humidity conditions will be expected to influence the LbL growth processes. In this study, we fabricated MOF thin films composed of Zn^{2+} , tetrakis-(4-carboxyphenyl)-porphyrin (TCPP), and 4,4'-bipyridyl (bpy) at 10% and 40% relative humidity (RH) conditions. Then we investigated the humidity effects on chemical compositions of TCPP and bpy, periodic structure, orientation, and surface morphology. At high RH, coordination replacement of water with the organic linkers becomes more competitive than that at low RH, resulting in a different TCPP:bpy composition ratio between the two RH conditions. Also, more frequent coordination replacements of water with the organic linkers at high RH led to formation of phases other than that observed at low RH, loss of growth orientation and rough surface. The findings clarified the importance of controlling RH condition during LbL growth to obtain the desired coordination networks.

1. Introduction

Metal–organic frameworks (MOFs) are hybrid and periodic nanoporous materials composed of metal ion/metal oxide clusters connected with organic linkers.^{1–3} The pore sizes and pore dimensions can be designed by choosing the appropriate combination of secondary building units (SBUs)^{4–6} and organic linkers. MOFs are promising materials for use in selective gas absorption and separation,^{7–12} catalysts,^{12–17} luminescence,^{18–21} ion transport,^{22–27} and so on. Especially, development of MOF thin film assemblies is an essential technique for applications involving membranes and nanodevices, such as chemical sensing,^{28–30} photovoltaics^{31,32} and fuel cells.^{33–35} Using bottom-up methods, the growth direction and the rate of the thin assembly films can be controlled.^{36–39} Well-ordered MOF thin films are fabricated by various methods such as layer-by-layer (LbL) method,^{40–43} Langmuir–Blodgett/Langmuir–Schäfer methods,^{44–46} surfactant-assisted approaches,^{47,48} and others.^{49–51}

Porphyrin derivatives are intensively studied functional organic linkers in MOF thin film assemblies.^{52–56} They are desirable for applications such as catalysts,^{57–59} light harvesting,^{60–63} and sensors.^{64–67} Hupp, Farha and coworkers reported syntheses of MOF thin films consisting of Zn²⁺, tetrakis-(4-carboxyphenyl)-porphyrin (TCPP), and 4,4'-bipyridyl (bpy) by LbL method on SiO₂ substrates.^{68,69} They proposed that the obtained films adopted paddlewheel-type Zn-TCPP coordination networks based on XRD results and reports of the literature.⁷⁰ One salient feature of this MOF thin film is that bpy can be replaced with pyridine vapor in a post-synthetic manner: solvent-assisted linker exchange (SALE).⁷¹ This coordination replacement led to structural change and

enhanced energy transfer ability.⁷¹ Considering the coordination ability, other solvents such as water in the air can also compete with the replacement reaction. The coordination competition and replacement of the water with the organic linker has often been observed during bulk MOF syntheses.⁷²⁻⁷⁴ Nevertheless, no report describes an investigation of the influence of humidity during MOF thin film fabrication on the LbL growth manner or the structure.

In this study, MOF thin films consisting of Zn^{2+} ion, bpy, and TCPP were synthesized on the surface-modified SiO_2 substrate under low (10%, **1L**) and high (40%, **1H**) relative humidity (RH) conditions using LbL method (Figure 1), and the influences of humidity on LbL growth and structure were examined. The TCPP:bpy chemical composition ratio of **1L** was nearly 1:1; it was consistent with the ideal chemical formula $[Zn_2(TCPP)(bpy)]$,⁶⁸ whereas that of **1H** was clearly distinct from 1:1 because of the enhanced coordination replacement and competition of water with organic linkers. This difference of the chemical composition influenced the periodic structure and orientation of the thin film. In **1L**, $[Zn_2(TCPP)(bpy)]$ single-phase material was obtained with in-plane orientation of the Zn-TCPP coordination network, as schematically shown in Figure 1(c). In contrast, because of the enhanced coordination replacement of organic linkers in **1H**, water inhibits construction of the $[Zn_2(TCPP)(bpy)]$ phase and loss of the orientation was observed (Figure 1(d)). Moreover, the high RH condition led to the rough and heterogeneous surface. Our study demonstrates the importance of humidity control during MOF thin film fabrication to obtain the desired phase and surfaces for application in nanodevices.

2. Experimental Section

For the LbL growth of MOF thin films, the quartz substrate ($25 \times 15 \times 0.5$ mm³) was first cleaned twice using 2-propanol with sonication for 10 min. Then, to form the self-assembled monolayer (SAM), the substrate was immersed in a 10 mM ethanol solution of 3-aminopropyltrimethoxysilane (APTMS) at room temperature for 1 h under an Ar atmosphere with mild shaking. Next, the substrate was immersed in 2-propanol with sonication for 30 min. To fabricate the MOF thin films under controlled RH conditions, a homemade humidity-controllable box using the saturated NaCl (aq) and N₂ gas flow was developed (See SI for details). Inside the RH-controlled box, the SAM-modified substrate was alternately immersed into 100 μM ethanol solution of Zn(CH₃COO)₂·2H₂O for 5 min, 2 μM ethanol solution of TCPP for 10 min, and 20 μM ethanol solution of bpy for 10 min (Figure 1). After each immersion step, the substrate was washed thoroughly with ethanol and dried. The desired number of layers by the alternate deposition of Zn²⁺ ion and two organic linkers is defined as “*n*” layers, denoted as (1L)_{*n*} or (1H)_{*n*}.

To investigate the influence of humidity on LbL growth, ultraviolet visible (UV-vis) spectroscopy was conducted for (1L)_{*n*} and (1H)_{*n*} in absorption mode using a UV-Vis spectrophotometer (JASCO V-630Bio; Jasco Corp., Japan) at room temperature. Measurements were taken at 300–800 nm with the step of 1.0 nm. To elucidate the chemical composition, X-ray photoelectron spectroscopy (XPS) was conducted using a delay-line detector (DLD) spectrometer (Kratos Axis-Ultra; Kratos Analytical Ltd., UK) with an Al *K*α radiation source (1486.6 eV) and the

respective voltage and current of 15 kV and 10 mA. The conductive carbon tape was attached to the sample. Each spectrum was calibrated to the C 1s peak at 284.5 eV as the inner reference. The obtained spectra were fitted using XPSPEAK 4.1 software with subtraction of the background using the Shirley method. Grazing-incidence X-ray scattering (GI-XRS) measurements were performed to analyze the periodic structure and the orientation of the MOF thin films using an X-ray diffractometer (FR-E; Rigaku Corp., Japan) with a two-dimensional (2D) detector (R-AXIS IV; Rigaku Corp., Japan). The film sample was placed onto a pulse motor stage composed of an oblique pulse (ATS-C316-EM; Chuo Precision Industrial Co. Ltd., Japan) and a Z-pulse (ALV-300-HM; Chuo Precision Industrial Co. Ltd., Japan) motor. The Cu $K\alpha$ radiation source ($\lambda = 0.1542$ nm) was used with ϕ 300 μm beam size and 300 mm camera length. The incident angle of the X-ray beam was adjusted to 0.21° or 0.22° to the substrate surface using the pulse motors. One-dimensional (1D) diffraction patterns of in-plane (IP), out-of-plane (OP), and 30, 50, and 70 degrees from the IP direction were obtained from the 2D image using ImageJ software. Le Bail fitting of these diffraction patterns was conducted using TOPAS3 (Bruker AXS). An atomic force microscope (AFM) was used to observe the surface morphology and roughness of the thin films. The AFM (MMAFM-2; Veeco Instruments, USA) measurements were taken in the range of $1 \times 1 \mu\text{m}^2$. The root mean square roughness was analyzed using WSxM 5.0 software. X-ray reflectivity (XRR) measurements were used to characterize the film thickness and roughness using the X-ray diffractometer (ATX-G; Rigaku Corp., Japan) at 50 kV

voltage and 300 mA current with Cu $K\alpha$ radiation ($\lambda = 0.1542$ nm). Data acquisition was performed at intervals of 0.02° between $0-2^\circ$. Fitting was conducted using GenX 3.

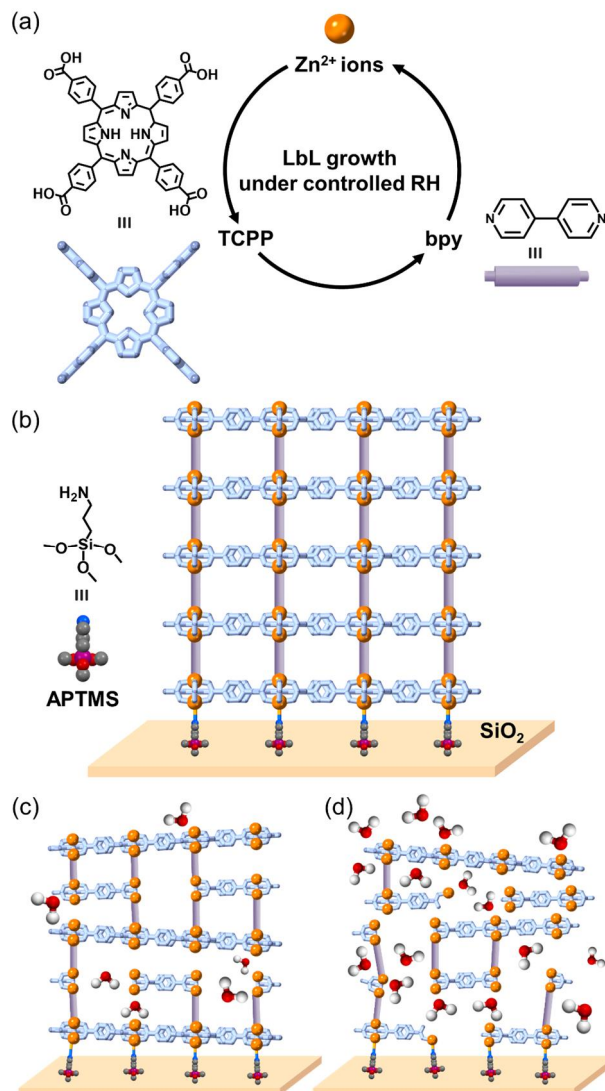


Figure 1. (a) LbL growth of MOF thin film composed of Zn²⁺ ions, TCPP and bpy under humidity controlled condition. (b) to (d) Schematic images of (b) ideal MOF thin film structure [Zn₂(TCPP)(bpy)] and obtained MOF thin film structure synthesized at (c) 10% RH and (d) 40% RH on APTMS-modified SiO₂ substrate.

3. Results and Discussion

3.1. Humidity effects on LbL growth by UV-vis spectra

The MOF thin films (**1L**)_n and (**1H**)_n were fabricated using LbL growth at 10% and 40% RH conditions, respectively. Figures 2a and 2b respectively depict the UV-vis spectra of (a) (**1L**)_n and (b) (**1H**)_n (number of layers $n = 1, 5, 10, 15, 20$). For all spectra, the absorption bands corresponding to the Soret band and Q-band from TCPP were observed respectively at 420 nm and 500–650 nm. The Soret band position did not shift as n increases, while a red shift was observed for the Q-bands (Figure S3 and Table S1). Figure 2c depicts the peak top of the Soret band of (**1L**)_n (red) and (**1H**)_n (blue). At each layer, the absorbance of the Soret band in (**1L**)_n was greater than that in (**1H**)_n, indicating that coordination competition and replacement of TCPP with water occurred more often at 40% RH. The absorbance of these bands increased linearly with n , except for the first deposition ($n = 1$), which suggests that the TCPP linker is deposited a bit more in the first layer and that it contains approximately equal amounts of TCPP at each layer during LbL growth. The slope in Figure 2c of (**1L**)_n (0.031 ± 0.001) was 1.2 times greater than that of (**1H**)_n (0.025 ± 0.001). Similar trends were observed for those of Q-bands (Figure S3 and Table S2). These results clearly suggest that humidity affects LbL growth and the TCPP contents at each deposition step.

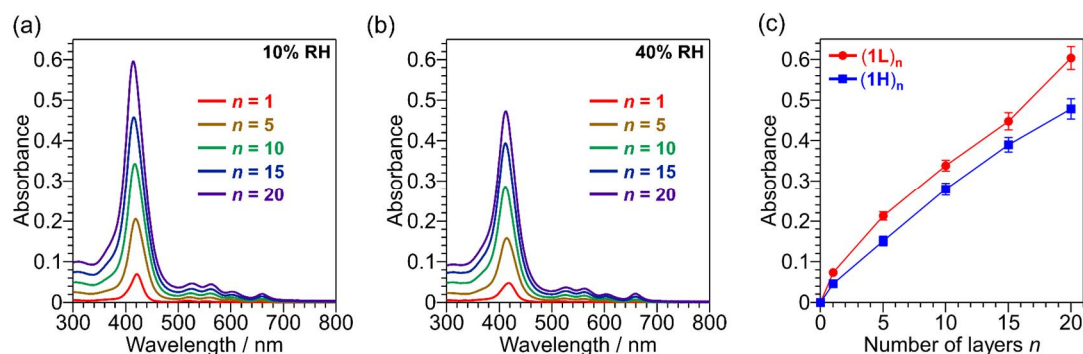


Figure 2. (a) and (b) UV-vis absorption spectra of (a) $(\mathbf{1L})_n$ and (b) $(\mathbf{1H})_n$ ($n = 1, 5, 10, 15, 20$) thin films. (c) Layer number n dependence of the Soret band absorbance of $(\mathbf{1L})_n$ (red) and $(\mathbf{1H})_n$ (blue).

The error bars represent the standard deviation of triplicates.

3.2. Analysis of chemical compositions using XPS

To get insights into the composition ratio and the coordination of bpy and TCPP with Zn^{2+} or H^+ , N 1s XPS was carried out. Figure 3a shows the N 1s XPS spectrum of the $(\mathbf{1L})_5$ thin film. The deconvolution was conducted considering the different chemical environment: four components for TCPP (non-coordinated species; P1 (=N-) and P2 (-NH), coordinated to H^+ ; P3 (=NH⁺-), and coordinated to Zn^{2+} ions; P4 (Zn-N), Figure S4)^{53,75-77}, one component for bpy (coordinated to Zn^{2+} ions; D1 (Zn-N), Figure S5), and two components for APTMS (NH₂ and NH₃⁺)^{78,79}. Table 1 presents the binding energy, area ratio and composition ratio of the peaks of TCPP (See SI for the deconvolution process). Based on the ideal chemical composition of the MOF thin film, $[\text{Zn}_2(\text{TCPP})(\text{bpy})]$, the expected composition ratio should be TCPP:bpy = 1:1. In $(\mathbf{1L})_5$, the observed composition ratio was calculated as TCPP:bpy = 0.48:0.52, which is nearly consistent with the ideal

[Zn₂(TCPP)(bpy)] structure. The structural consistency of **1L** and [Zn₂(TCPP)(bpy)] was supported further by GI-XRD measurement, *vide infra*. Figure 3b shows N 1s XPS spectrum and the deconvoluted result of (**1H**)₅ thin film. Judging from the area ratio of P4 (Zn–N) component of TCPP (Table 2), we found that Zn²⁺ ions were partially inserted into the TCPP center in both humidity conditions (14% of TCPP for (**1L**)₅ and 10% of TCPP for (**1H**)₅), although -COO⁻ groups preferably coordinate to Zn²⁺ ions rather than the center of TCPP. It is noteworthy that the TCPP:bpy composition ratio of the (**1H**)₅ was calculated to be 0.76:0.24, which differs greatly from 1:1. The relative amount of bpy decreased distinctly at 40% RH, suggesting that bpy was replaced more easily with water than TCPP,⁴⁸ although replacement of TCPP with water also occurred, as revealed by UV-vis. From the analysis described above, it is indicated that the humidity clearly affects LbL growth; namely the chemical composition of organic linkers due to coordination competition and replacement.

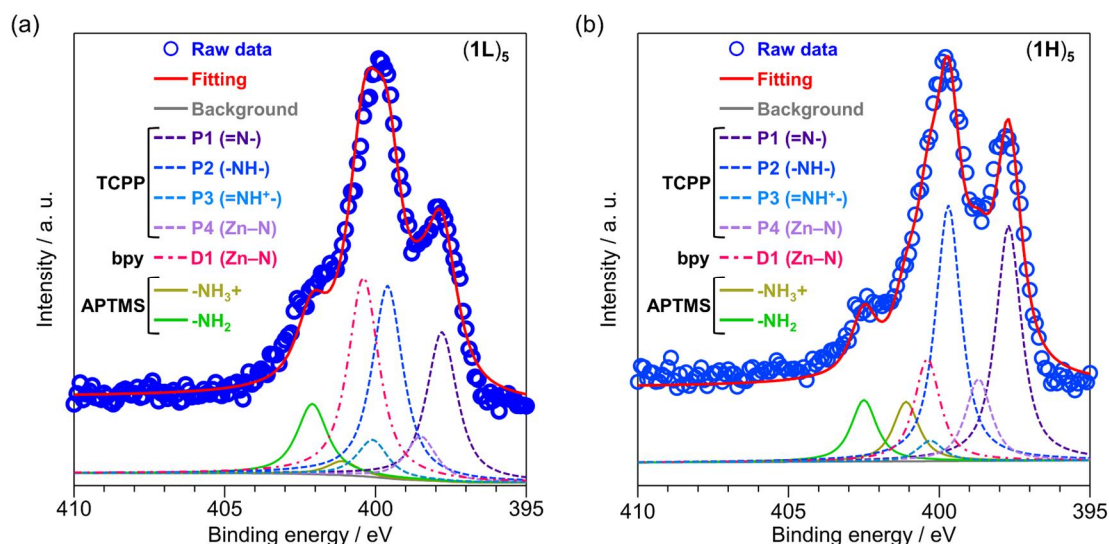


Figure 3. Respective N 1s XPS spectra and fitting results of (a) (**1L**)₅ and (b) (**1H**)₅ thin films.

Table 1 Peak deconvolution results of N1s XPS spectra of (1L)₅ and (1H)₅ thin films

Entry	Compound	Assignment	Binding energy / eV	Area ratio	TCPP: bpy composition ratio
(1L) ₅	TCPP	P1 (=N-)	397.8	0.24	0.52
		P2 (-NH-)	399.6	0.31	
		P3 (=NH ⁺ -)	400.1	0.06	
		P4 (Zn-N)	398.5	0.07	
	bpy	D1 (Zn-N)	400.4	0.32	0.48
	APTMS	NH ₂	402.1	0.94	-
NH ₃ ⁺		401.1	0.06		
(1H) ₅	TCPP	P1 (=N-)	397.7	0.34	0.74
		P2 (-NH-)	399.7	0.37	
		P3 (=NH ⁺ -)	400.3	0.03	
		P4 (Zn-N)	398.7	0.12	
	bpy	D1 (Zn-N)	400.4	0.15	0.26
	APTMS	NH ₂	402.5	0.51	-
NH ₃ ⁺		401.1	0.49		

3.3. Humidity effects on the structure by GI-XRS profiles

GI-XRS measurements were conducted to evaluate the periodic structure and orientation of the MOF thin film. Figure 4a shows the 2D GI-XRS profile of the (1L)₂₅ thin film. Figures 4d and 4e respectively portray its 1D projected profiles to the (d) IP and (e) OP directions. Two peaks were observed at $d = 1.7$ nm ($2\theta = 5.2^\circ$) and 1.2 nm ($2\theta = 7.5^\circ$) in the IP direction, whereas no peak was observed for the OP direction, indicating the construction of the periodic coordination network in the IP direction. In an earlier report, Hupp and coworkers proposed that the obtained thin film has a Zn-TCPP paddlewheel-type structure.⁶⁸ The thin film examined for their study showed no IP scattering, while only one OP scattering corresponding to the interlayer length ($d = 1.4$ nm) was observed. Instead of the absence of the IP information, they identified the film orientation using polarized

fluorescence measurements. In our study, the IP network structure based on the paddlewheel-type structure was supported by these two peaks. Figures 4b and 4c show our model structure of the paddlewheel-type coordination network $[\text{Zn}_2(\text{TCPP})(\text{bpy})]$. A unit cell of the coordination network was created using Materials Studio 2018 under the conditions of $a = b = 1.70$ nm, $c = 1.40$ nm (space group $P4/mmm$, see SI for details of the space group determination) based on single-crystal structural analysis result of the similar bulk structure.⁸⁰ The Zn^{2+} dimers coordinated with four $-\text{COO}^-$ groups of TCPP form the paddle-wheel type 2D layer in the ab plane (Figure 4b), and bpy molecules bridge 2D layers coordinating to apical position of Zn^{2+} ions (Figure 4c). We ignored the Zn^{2+} insertion to the center of TCPP because of the low content, confirmed by XPS. Using Le Bail fitting of the IP diffraction pattern, cell parameter $a (= b)$ of $(\mathbf{1L})_{25}$ was fitted to be 1.6775(7) nm, which is consistent with structural analysis results report⁸⁰. Two scattering peaks correspond to the 100 and 110 diffractions, and the intensity ratio of these two diffractions were in good agreement with the simulated patterns from the model structure. Unfortunately, cell parameter c along the pillar direction could not be fitted because of the fluctuated structure. Our study demonstrates that paddlewheel-type coordination network extends periodically in IP direction, although periodic structure is hardly observed in OP direction in $(\mathbf{1L})_{25}$.

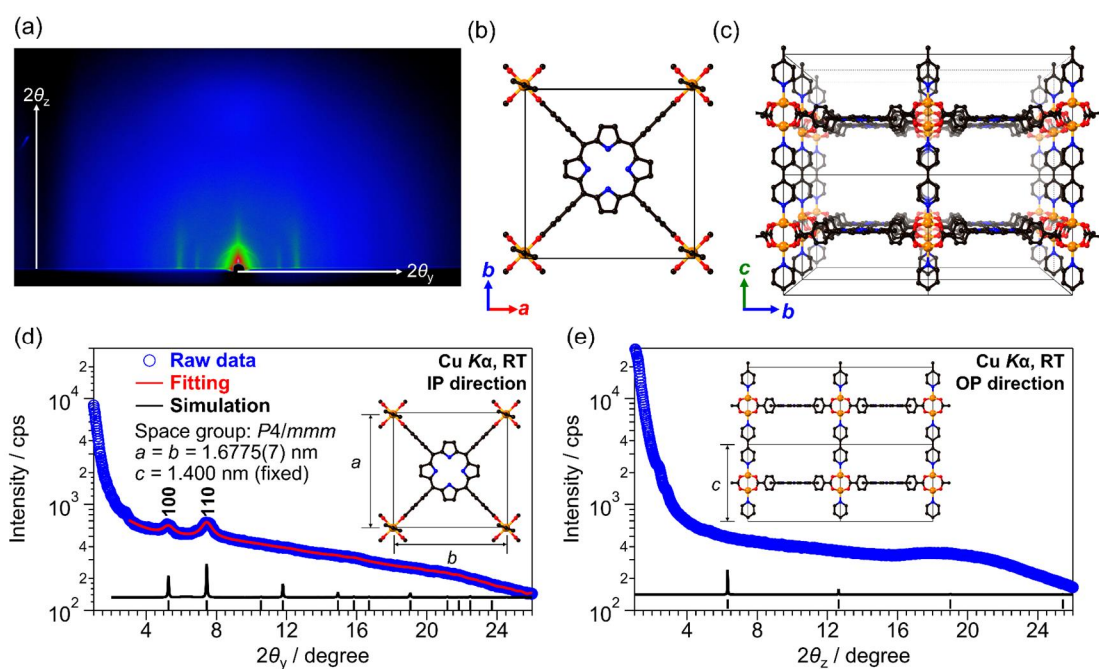


Figure 4. (a) 2D GI-XRS image of (1L)₂₅ thin film. (b) and (c) Constructed model structure of [Zn₂(TCPP)(bpy)] under the space group *P4/mmm* viewed along (b) *c*-axis and (c) *a*-axis, respectively (orange, Zn; red, O; blue, N; black, C). H atoms are omitted for clarity. Panels (d) and (e) respectively portray 1D projected of panel (a) in (d) IP direction and Le Bail fitting results, and (e) OP direction. Black ticks correspond to *hk0* and *00l* diffractions of the simulated patterns, respectively.

On the other hand, a complicated Debye-ring-like scattering pattern was observed in the 2D GI-XRS image of the (1H)₂₅ thin film (Figure 5a), indicating the polycrystalline nature and the loss of the specific orientation of the coordination network. In the IP (Figure 5b) and OP (Figure 5c) projected patterns, 100 ($2\theta = 5.2^\circ$) scattering was observed in both directions, while 110 ($2\theta = 7.5^\circ$) scattering peak, which was observed in the thin film synthesized at 10% RH, was not detected. Instead, two peaks were observed at $d = 1.3$ nm ($2\theta = 6.9^\circ$) and 1.1 nm ($2\theta = 8.1^\circ$) in both the IP and OP directions. Considering the polycrystalline nature, we performed Le Bail fitting for refining both $a (= b)$ and c

(Figures 5b and 5c), resulting in $a = 1.679(1)$ nm ($1.701(1)$ nm) and $c = 1.287(1)$ nm ($1.302(2)$ nm), respectively, for the IP (OP) directions. The obtained cell parameters do not match and contain unidentified peaks (black triangles in Figures 5b and 5c), and the experimental intensity ratios are inconsistent with the those of the simulated patterns. We also conducted fitting to the 1D projected patterns between IP and OP (Figure S7). The unidentified peaks were observed in all fitting results, and the fitted cell parameters are not mutually consistent. These XRS analyses results indicate clear structural differences between $(\mathbf{1L})_{25}$ and $(\mathbf{1H})_{25}$; the amount of water in air during synthesis affects the orientation and the structure. In $(\mathbf{1L})_{25}$, because the water content in the air was suppressed, organic linkers were coordinated preferentially to the Zn^{2+} ions to give the $[\text{Zn}_2(\text{TCPP})(\text{bpy})]$ coordination network with the IP orientation. By contrast, in $(\mathbf{1H})_{25}$, water competes with TCPP and bpy in coordination to the Zn^{2+} ions, leading to the formation of phases other than $[\text{Zn}_2(\text{TCPP})(\text{bpy})]$ and to the loss of orientation. Especially, bpy was replaced preferentially with water supported from XPS. Therefore, one of the expected phases will be the structure where water occupies the apical position and Zn-TCPP layer stack in the interdigitated manner. While OP scattering was absent in $(\mathbf{1L})_{25}$ due to the fluctuated nature along this direction, several peaks appeared in the OP direction in $(\mathbf{1H})_{25}$. This was derived from polycrystalline $[\text{Zn}_2(\text{TCPP})(\text{bpy})]$ (including IP scatterings in $(\mathbf{1L})_{25}$) due to the loss of specific orientation. Also, since we could not fit the scatterings with $[\text{Zn}_2(\text{TCPP})(\text{bpy})]$ structure, scattering from other phases were observed. Results indicate that it is necessary to suppress water vapor generation, *i.e.* humidity, to synthesize the $[\text{Zn}_2(\text{TCPP})(\text{bpy})]$

coordination network in a single phase.

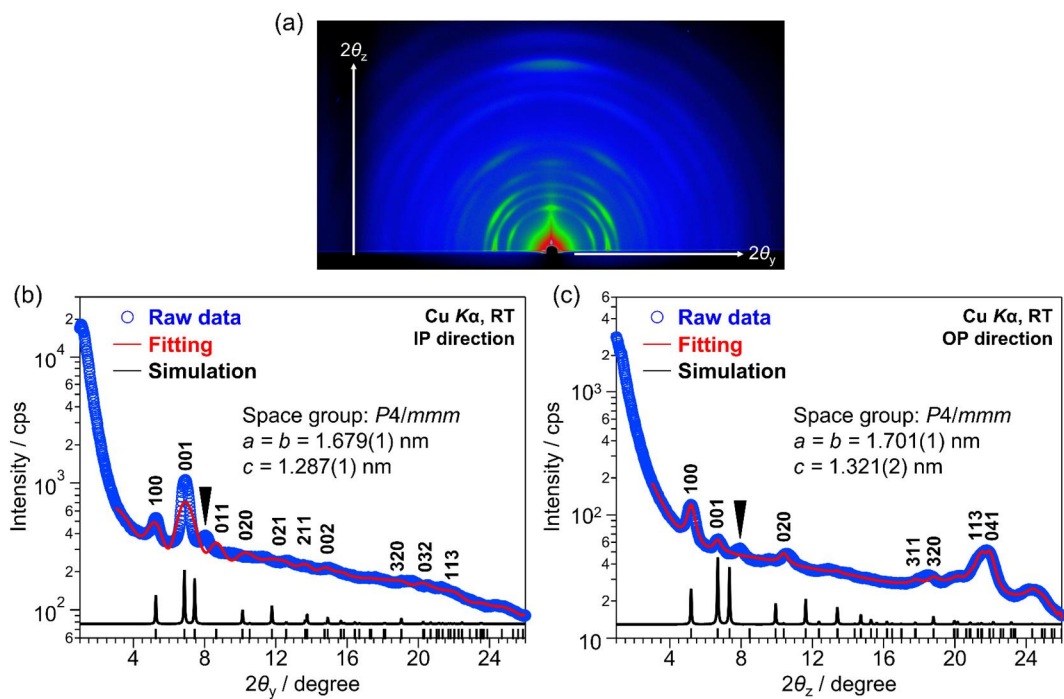


Figure 5. (a) 2D GI-XRS image of $(1\mathbf{H})_{25}$ thin film. Panels (b) and (c) respectively portray 1D projected patterns of panel (a) in (b) IP and (c) OP directions, along with their fitting results and simulated patterns. The black ticks correspond to hkl diffractions. The black triangles represent the unidentified peaks.

3.4 Humidity effects on surface morphology by AFM and XRR analyses

To investigate humidity effects on surface morphologies, AFM was carried out. Figures 6a to 6d respectively show AFM images of (a) $(\mathbf{1L})_5$, (b) $(\mathbf{1L})_{25}$, (c) $(\mathbf{1H})_5$ and (d) $(\mathbf{1H})_{25}$ thin films, and Table 2 presents the root mean square (RMS) roughness values of the thin films. Homogeneous and relatively small (10-20 nm) islands were observed in $(\mathbf{1L})_5$, and these small islands grew and merged to form a smooth surface with negligible islands or domains in $(\mathbf{1L})_{25}$ (Figure 6(c)). This observation was consistent with the previous study.⁶⁸ In contrast to $(\mathbf{1L})_5$, inhomogeneous domains (20-100 nm and height of *ca.* 10 nm) and rough surface (5.8 nm RMS roughness) were already formed for $(\mathbf{1H})_5$ (Figure 6(c)). This was consistent with the XPS result in Figure 3, where the water replaces the ligand and inhibits the uniform growth of MOF thin film. As the layer number increased, the inhomogeneous domains retained with a grown domain height of *ca.* 50 nm in $(\mathbf{1H})_{25}$. This inhomogeneity led to the loss of specific orientation and contamination of other phases than $[\text{Zn}_2(\text{TCPP})(\text{bpy})]$, from GI-XRS (Figure 5). To further investigate the surface roughness in large areas, XRR was applied to $(\mathbf{1L})_{25}$ and $(\mathbf{1H})_{25}$ thin films (Figure 6(e) and (f)). Clear fringes were observed in $(\mathbf{1L})_{25}$, whereas no fringe was detected in $(\mathbf{1H})_{25}$, thereby reflecting the rougher surface of the thin film synthesized at higher RH. Fitting was conducted for $(\mathbf{1L})_{25}$, and the estimated surface roughness (3.5 nm) showed close agreement with the AFM result (3.0 nm). The fitted thickness was 21.3 nm, corresponding to 0.85 nm deposition per cycle. This was inconsistent with the ideal MOF structure (1.4 nm), because of the fluctuated nature along the OP direction from GI-XRS (Figure 4(e)). The findings indicated the clear

influence of humidity on the growth manner of the MOF thin film, and the importance of the RH control to produce a MOF thin film with a smooth surface.

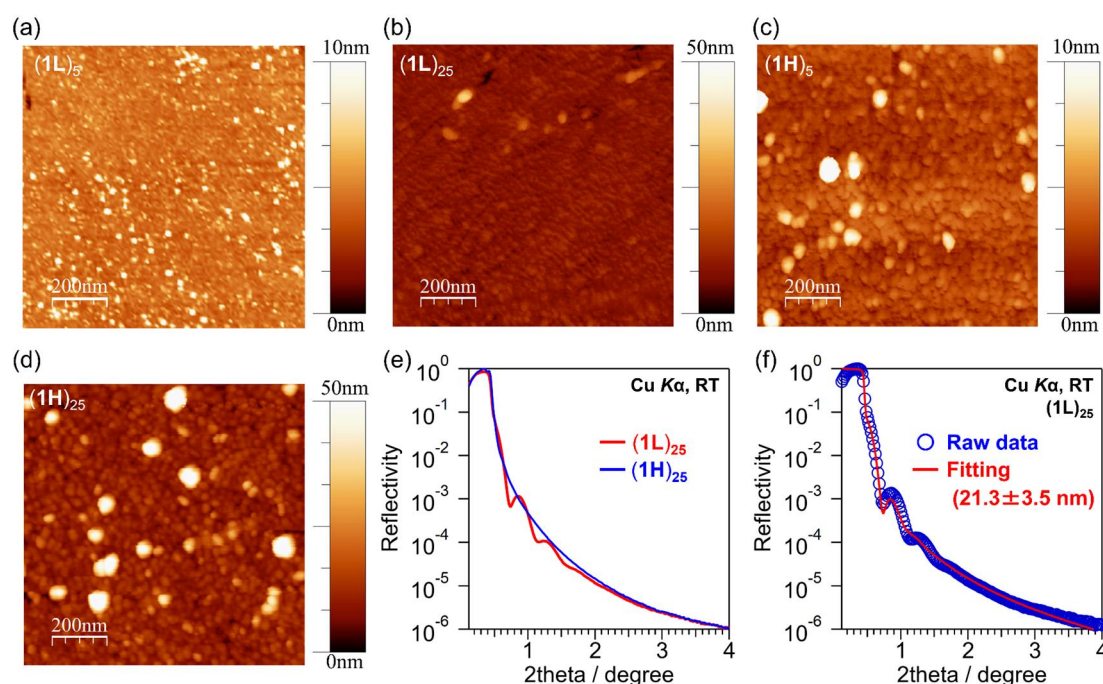


Figure 6. (a) to (d) AFM images of (a) $(1L)_5$, (b) $(1L)_{25}$, (c) $(1H)_5$ and (d) $(1H)_{25}$. (e) XRR spectra of $(1L)_{25}$ (red) and $(1H)_{25}$ (blue), and (f) fitting result of $(1L)_{25}$.

Table 2 Surface roughness of $(1L)_5$, $(1H)_5$, $(1L)_{25}$ and $(1H)_{25}$ thin films estimated from AFM.

Entry	RMS roughness / nm
$(1L)_5$	1.2
$(1H)_5$	5.8
$(1L)_{25}$	3.0
$(1H)_{25}$	7.3

4. Conclusion

In this study, we fabricated the MOF thin films composed Zn^{2+} ions and two organic linkers (bpy and TCPP) using LbL method under different RH conditions, and its influence was investigated. Organic linkers (especially bpy molecules) were replaced with water more frequently at higher RH than at lower RH, thereby producing a change in the TCPP:bpy ratio. This difference of chemical

compositions at high RH caused contamination of the phase other than that observed at low RH, [Zn₂(TCPP)(bpy)] phase. In addition, coordination replacement of water with organic linkers loses the structural orientation on the substrate, as well as the rough surfaces. Our findings demonstrate the importance of controlling humidity to achieve the desired structure and surface morphology during LbL growth.

ASSOCIATED CONTENT

Supporting Information. Supporting Information is available free of charge at <http://pubs.acs.org>. RH control method during the LbL growth, UV-vis in the Q-band region, XPS of organic linkers and peak deconvolution method, space group estimation for GI-XRS and its fitting result including Figures S1–S7 and Tables S1–S5 (PDF).

AUTHOR INFORMATION

Corresponding Author

*Email: ynagao@jaist.ac.jp

ORCID

Kentaro Aoki: 0000-0003-4148-6070

Mitsuo Hara: 0000-0003-1829-5153

Shusaku Nagano: 0000-0002-3929-6377

Yuki Nagao: 0000-0003-1249-440X

ACKNOWLEDGMENTS

We are grateful to Prof. Yukiko Yamada-Takamura and Dr. Takahiro Yonezawa of the Japan Advanced Institute for Science and Technology for their support with AFM measurements. This work was supported by research funding from JSPS KAKENHI Grant Number JP22K20555, The Murata Science Foundation, and JST CREST Grant Number JPMJCR21B3. This work was supported in part by the Nanotechnology Platform Program (Molecule and Material Synthesis) of the Ministry of Education, Culture, Sports, Science and Technology (MEXT), Japan.

Notes

The authors declare no competing financial interest.

5. References

- (1) Yaghi, O. M. Reticular Chemistry – Construction, Properties, and Precision Reactions of Frameworks. *J. Am. Chem. Soc.* **2016**, *138*, 15507–15509.
- (2) Öhrström, L.; Amombo Noa, F. M. *Metal–Organic Frameworks*; ACS In Focus; American Chemical Society: Washington, DC, USA, 2021.
- (3) Kaskel, S. *The Chemistry of Metal–Organic Frameworks: Synthesis, Characterization, and Applications*; Wiley-VCH: Weinheim, 2016.
- (4) Tranchemontagne, D. J.; Mendoza-Cortés, J. L.; O’Keeffe, M.; Yaghi, O. M. Secondary Building Units, Nets and Bonding in the Chemistry of Metal–Organic Frameworks. *Chem. Soc. Rev.* **2009**, *38*, 1257–1283.

- (5) Kalmutzki, M. J.; Hanikel, N.; Yaghi, O. M. Secondary Building Units as the Turning Point in the Development of the Reticular Chemistry of MOFs. *Sci. Adv.* **2018**, *4*, eaat9180.
- (6) Guo, J.; Xue, X.; Yu, H.; Duan, Y.; Li, F.; Lian, Y.; Liu, Y.; Zhao, M. Metal–Organic Frameworks Based on Infinite Secondary Building Units: Recent Progress and Future Outlooks. *J. Mater. Chem.* **2022**, *10*, 19320–19347.
- (7) Li, J.-R.; Kuppler, R. J.; Zhou, H.-C. Selective Gas Adsorption and Separation in Metal–Organic Frameworks. *Chem. Soc. Rev.* **2009**, *38*, 1477–1504.
- (8) Li, J.-R.; Sculley, J.; Zhou, H.-C. Metal–Organic Frameworks for Separations. *Chem. Rev.* **2012**, *112*, 869–932.
- (9) Sumida, K.; Rogow, D. L.; Mason, J. A.; McDonald, T. M.; Bloch, E. D.; Herm, Z. R.; Bae, T.-H.; Long, J. R. Carbon Dioxide Capture in Metal–Organic Frameworks. *Chem. Rev.* **2012**, *112*, 724–781.
- (10) Fan, W.; Zhang, X.; Kang, Z.; Liu, X.; Sun, D. Isostructural Chemistry within Metal–Organic Frameworks for Gas Storage and Separation. *Coord. Chem. Rev.* **2021**, *443*, 213968.
- (11) Kang, D.-Y.; Lee, J. S.; Lin, L.-C. X-Ray Diffraction and Molecular Simulations in the Study of Metal–Organic Frameworks for Membrane Gas Separation. *Langmuir* **2022**, *38*, 9441–9453.
- (12) Farrusseng, D. *Metal–Organic Frameworks: Applications from Catalysis to Gas Storage*; John Wiley & Sons, 2011.
- (13) Lee, J.; Farha, O. K.; Roberts, J.; Scheidt, K. A.; Nguyen, S. T.; Hupp, J. T. Metal–Organic

- Framework Materials as Catalysts. *Chem. Soc. Rev.* **2009**, *38*, 1450–1459.
- (14) Dhakshinamoorthy, A.; Li, Z.; Garcia, H. Catalysis and Photocatalysis by Metal Organic Frameworks. *Chem. Soc. Rev.* **2018**, *47*, 8134–8172.
- (15) Konnerth, H.; Matsagar, B. M.; Chen, S. S.; Precht, M. H. G.; Shieh, F.-K.; Wu, K. C.-W. Metal–Organic Framework (MOF)-Derived Catalysts for Fine Chemical Production. *Coord. Chem. Rev.* **2020**, *416*, 213319.
- (16) Wang, Q.; Astruc, D. State of the Art and Prospects in Metal–Organic Framework (MOF)-Based and MOF-Derived Nanocatalysis. *Chem. Rev.* **2020**, *120*, 1438–1511.
- (17) Gulati, S. *Metal–Organic Frameworks (MOFs) as Catalysts*; Springer Nature Singapore, 2022.
- (18) Allendorf, M. D.; Bauer, C. A.; Bhakta, R. K.; Houk, R. J. T. Luminescent Metal–Organic Frameworks. *Chem. Soc. Rev.* **2009**, *38*, 1330–1352.
- (19) Cui, Y.; Yue, Y.; Qian, G.; Chen, B. Luminescent Functional Metal–Organic Frameworks. *Chem. Rev.* **2012**, *112*, 1126–1162.
- (20) Lustig, W. P.; Mukherjee, S.; Rudd, N. D.; Desai, A. V.; Li, J.; Ghosh, S. K. Metal–Organic Frameworks: Functional Luminescent and Photonic Materials for Sensing Applications. *Chem. Soc. Rev.* **2017**, *46*, 3242–3285.
- (21) Whelan, É.; Steuber, F. W.; Gunnlaugsson, T.; Schmitt, W. Tuning Photoactive Metal–Organic Frameworks for Luminescence and Photocatalytic Applications. *Coord. Chem. Rev.* **2021**,

437, 213757.

- (22) Horike, S.; Umeyama, D.; Kitagawa, S. Ion Conductivity and Transport by Porous Coordination Polymers and Metal–Organic Frameworks. *Acc. Chem. Res.* **2013**, *46*, 2376–2384.
- (23) Ramaswamy, P.; Wong, N. E.; Shimizu, G. K. H. MOFs as Proton Conductors – Challenges and Opportunities. *Chem. Soc. Rev.* **2014**, *43*, 5913–5932.
- (24) Yamada, T. Proton Conductive Metal–Organic Frameworks. *Bull. Chem. Soc. Jpn.* **2013**, *61*, 46–54.
- (25) Ye, Y.; Gong, L.; Xiang, S.; Zhang, Z.; Chen, B. Metal–Organic Frameworks as a Versatile Platform for Proton Conductors. *Adv. Mater.* **2020**, *32*, 1907090.
- (26) Zhang, G.; Jin, L.; Zhang, R.; Bai, Y.; Zhu, R.; Pang, H. Recent Advances in the Development of Electronically and Ionically Conductive Metal–Organic Frameworks. *Coord. Chem. Rev.* **2021**, *439*, 213915.
- (27) Lim, D.-W.; Kitagawa, H. Rational Strategies for Proton-Conductive Metal–Organic Frameworks. *Chem. Soc. Rev.* **2021**, *50*, 6349–6368.
- (28) Kreno, L. E.; Leong, K.; Farha, O. K.; Allendorf, M.; Van Duyne, R. P.; Hupp, J. T. Metal–Organic Framework Materials as Chemical Sensors. *Chem. Rev.* **2012**, *112*, 1105–1125.
- (29) Zhang, Y.; Yuan, S.; Day, G.; Wang, X.; Yang, X.; Zhou, H.-C. Luminescent Sensors Based on Metal–Organic Frameworks. *Coord. Chem. Rev.* **2018**, *354*, 28–45.
- (30) E. Ellis, J.; E. Crawford, S.; Kim, K.-J. Metal–Organic Framework Thin Films as Versatile

Chemical Sensing Materials. *Mater. Adv.* **2021**, *2*, 6169–6196.

- (31) Kaur, R.; Kim, K.-H.; Paul, A. K.; Deep, A. Recent Advances in the Photovoltaic Applications of Coordination Polymers and Metal Organic Frameworks. *J. Mater. Chem. A* **2016**, *4*, 3991–4002.
- (32) Chueh, C.-C.; Chen, C.-I.; Su, Y.-A.; Konnerth, H.; Gu, Y.-J.; Kung, C.-W.; Wu, K. C.-W. Harnessing MOF Materials in Photovoltaic Devices: Recent Advances, Challenges, and Perspectives. *J. Mater. Chem. A* **2019**, *7*, 17079–17095.
- (33) Yang, L.; Zeng, X.; Wang, W.; Cao, D. Recent Progress in MOF-Derived, Heteroatom-Doped Porous Carbons as Highly Efficient Electrocatalysts for Oxygen Reduction Reaction in Fuel Cells. *Adv. Funct. Mater.* **2018**, *28*, 1704537.
- (34) Wen, X.; Zhang, Q.; Guan, J. Applications of Metal–Organic Framework-Derived Materials in Fuel Cells and Metal–Air Batteries. *Coord. Chem. Rev.* **2020**, *409*, 213214.
- (35) Zhou, J.; Zeng, C.; Ou, H.; Yang, Q.; Xie, Q.; Zeb, A.; Lin, X.; Ali, Z.; Hu, L. Metal–Organic Framework-Based Materials for Full Cell Systems: A Review. *J. Mater. Chem. C* **2021**, *9*, 11030–11058.
- (36) Xu, G.; Yamada, T.; Otsubo, K.; Sakaida, S.; Kitagawa, H. Facile “Modular Assembly” for Fast Construction of a Highly Oriented Crystalline MOF Nanofilm. *J. Am. Chem. Soc.* **2012**, *134*, 16524–16527.
- (37) Otsubo, K.; Kitagawa, H. Metal–Organic Framework Thin Films with Well-Controlled

- Growth Directions Confirmed by X-ray Study. *APL Materials* **2014**, *2*, 124105.
- (38) Liu, J.; Wöll, C. Surface-Supported Metal–Organic Framework Thin Films: Fabrication Methods, Applications, and Challenges. *Chem. Soc. Rev.* **2017**, *46*, 5730–5770.
- (39) Gu, Z.-G.; Zhang, J. Epitaxial Growth and Applications of Oriented Metal–Organic Framework Thin Films. *Coord. Chem. Rev.* **2019**, *378*, 513–532.
- (40) Shekhah, O.; Wang, H.; Kowarik, S.; Schreiber, F.; Paulus, M.; Tolan, M.; Sternemann, C.; Evers, F.; Zacher, D.; Fischer, R. A.; Wöll, C. Step-by-Step Route for the Synthesis of Metal–Organic Frameworks. *J. Am. Chem. Soc.* **2007**, *129*, 15118–15119.
- (41) Shekhah, O.; Wang, H.; Strunskus, T.; Cyganik, P.; Zacher, D.; Fischer, R.; Wöll, C. Layer-by-Layer Growth of Oriented Metal Organic Polymers on a Functionalized Organic Surface. *Langmuir* **2007**, *23*, 7440–7442.
- (42) Borges, J.; Mano, J. F. Molecular Interactions Driving the Layer-by-Layer Assembly of Multilayers. *Chem. Rev.* **2014**, *114*, 8883–8942.
- (43) Wang, Z.; Wöll, C. Fabrication of Metal–Organic Framework Thin Films Using Programmed Layer-by-Layer Assembly Techniques. *Adv. Mater. Technol.* **2019**, *4*, 1800413.
- (44) Makiura, R.; Motoyama, S.; Umemura, Y.; Yamanaka, H.; Sakata, O.; Kitagawa, H. Surface Nano-Architecture of a Metal–Organic Framework. *Nat. Mater.* **2010**, *9*, 565–571.
- (45) Tsotsalas, M.; Umemura, A.; Kim, F.; Sakata, Y.; Reboul, J.; Kitagawa, S.; Furukawa, S. Crystal Morphology-Directed Framework Orientation in Porous Coordination Polymer Films and

- Freestanding Membranes via Langmuir–Blodgett. *J. Mater. Chem.* **2012**, *22*, 10159–10165.
- (46) Makiura, R. Creation of Metal–Organic Framework Nanosheets by the Langmuir–Blodgett Technique. *Coord. Chem. Rev.* **2022**, *469*, 214650.
- (47) Zhao, M.; Wang, Y.; Ma, Q.; Huang, Y.; Zhang, X.; Ping, J.; Zhang, Z.; Lu, Q.; Yu, Y.; Xu, H.; Zhao, Y.; Zhang, H. Ultrathin 2D Metal–Organic Framework Nanosheets. *Adv. Mater.* **2015**, *27*, 7372–7378.
- (48) Cao, F.; Zhao, M.; Yu, Y.; Chen, B.; Huang, Y.; Yang, J.; Cao, X.; Lu, Q.; Zhang, X.; Zhang, Z.; Tan, C.; Zhang, H. Synthesis of Two-Dimensional CoS_{1.097}/Nitrogen-Doped Carbon Nanocomposites Using Metal–Organic Framework Nanosheets as Precursors for Supercapacitor Application. *J. Am. Chem. Soc.* **2016**, *138*, 6924–6927.
- (49) Reboul, J.; Furukawa, S.; Horike, N.; Tsotsalas, M.; Hirai, K.; Uehara, H.; Kondo, M.; Louvain, N.; Sakata, O.; Kitagawa, S. Mesoscopic Architectures of Porous Coordination Polymers Fabricated by Pseudomorphic Replication. *Nat. Mater.* **2012**, *11*, 717–723.
- (50) Falcaro, P.; Okada, K.; Hara, T.; Ikigaki, K.; Tokudome, Y.; Thornton, A. W.; Hill, A. J.; Williams, T.; Doonan, C.; Takahashi, M. Centimetre-Scale Micropore Alignment in Oriented Polycrystalline Metal–Organic Framework Films via Heteroepitaxial Growth. *Nat. Mater.* **2017**, *16*, 342–348.
- (51) Crivello, C.; Sevim, S.; Graniel, O.; Franco, C.; Pané, S.; Puigmartí-Luis, J.; Muñoz-Rojas, D. Advanced Technologies for the Fabrication of MOF Thin Films. *Mater. Horizons* **2021**, *8*, 168–

178.

- (52) Makiura, R.; Kitagawa, H. Porous Porphyrin Nanoarchitectures on Surfaces. *Eur. J. Inorg. Chem.* **2010**, *2010*, 3715–3724.
- (53) Laokroekiat, S.; Hara, M.; Nagano, S.; Nagao, Y. Metal–Organic Coordination Network Thin Film by Surface-Induced Assembly. *Langmuir* **2016**, *32*, 6648–6655.
- (54) Zhang, X.; Wasson, M. C.; Shayan, M.; Berdichevsky, E. K.; Ricardo-Noordberg, J.; Singh, Z.; Papazyan, E. K.; Castro, A. J.; Marino, P.; Ajoyan, Z.; Chen, Z.; Islamoglu, T.; Howarth, A. J.; Liu, Y.; Majewski, M. B.; Katz, M. J.; Mondloch, J. E.; Farha, O. K. A Historical Perspective on Porphyrin-Based Metal–Organic Frameworks and Their Applications. *Coord. Chem. Rev.* **2021**, *429*, 213615.
- (55) Zhou, Z.; Mukherjee, S.; Warnan, J.; Li, W.; Wannapaiboon, S.; Hou, S.; Rodewald, K.; Rieger, B.; Weidler, P. G.; Wöll, C.; Fischer, R. A. Porphyrin Based Metal–Organic Framework Films: Nucleation and Growth. *J. Mater. Chem. A* **2020**, *8*, 25941–25950.
- (56) Rajasree, S. S.; Li, X.; Deria, P. Physical Properties of Porphyrin-Based Crystalline Metal-organic Frameworks. *Commun. Chem.* **2021**, *4*, 1–14.
- (57) Lin, S.; Diercks, C. S.; Zhang, Y.-B.; Kornienko, N.; Nichols, E. M.; Zhao, Y.; Paris, A. R.; Kim, D.; Yang, P.; Yaghi, O. M.; Chang, C. J. Covalent Organic Frameworks Comprising Cobalt Porphyrins for Catalytic CO₂ Reduction in Water. *Science* **2015**, *349*, 1208–1213.
- (58) Hod, I.; Sampson, M. D.; Deria, P.; Kubiak, C. P.; Farha, O. K.; Hupp, J. T. Fe-Porphyrin-

Based Metal–Organic Framework Films as High-Surface Concentration, Heterogeneous Catalysts for Electrochemical Reduction of CO₂. *ACS Catal.* **2015**, *5*, 6302–6309.

- (59) Harvey, P. D. Porphyrin-Based Metal- and Covalent-Organic Frameworks as Heterogeneous Nanosized Photocatalysts in Organic Synthesis. *J. Mater. Chem. C* **2021**, *9*, 16885–16910.
- (60) Aratani, N.; Kim, D.; Osuka, A. Discrete Cyclic Porphyrin Arrays as Artificial Light-Harvesting Antenna. *Acc. Chem. Res.* **2009**, *42*, 1922–1934.
- (61) Lee, C. Y.; Farha, O. K.; Hong, B. J.; Sarjeant, A. A.; Nguyen, S. T.; Hupp, J. T. Light-Harvesting Metal–Organic Frameworks (MOFs): Efficient Strut-to-Strut Energy Transfer in Bodipy and Porphyrin-Based MOFs. *J. Am. Chem. Soc.* **2011**, *133*, 15858–15861.
- (62) Son, H.-J.; Jin, S.; Patwardhan, S.; Wezenberg, S. J.; Jeong, N. C.; So, M.; Wilmer, C. E.; Sarjeant, A. A.; Schatz, G. C.; Snurr, R. Q.; Farha, O. K.; Wiederrecht, G. P.; Hupp, J. T. Light-Harvesting and Ultrafast Energy Migration in Porphyrin-Based Metal–Organic Frameworks. *J. Am. Chem. Soc.* **2013**, *135*, 862–869.
- (63) Schlachter, A.; Asselin, P.; Harvey, P. D. Porphyrin-Containing MOFs and COFs as Heterogeneous Photosensitizers for Singlet Oxygen-Based Antimicrobial Nanodevices. *ACS Appl. Mater. Interfaces* **2021**, *13*, 26651–26672.
- (64) Kung, C.-W.; Chang, T.-H.; Chou, L.-Y.; Hupp, J. T.; Farha, O. K.; Ho, K.-C. Porphyrin-Based Metal–Organic Framework Thin Films for Electrochemical Nitrite Detection. *Electrochem. Commun.* **2015**, *58*, 51–56.

- (65) Masih, D.; Chernikova, V.; Shekhah, O.; Eddaoudi, M.; Mohammed, O. F. Zeolite-like Metal–Organic Framework (MOF) Encaged Pt(II)-Porphyrin for Anion-Selective Sensing. *ACS Appl. Mater. Interfaces* **2018**, *10*, 11399–11405.
- (66) Hibbard, H. A. J.; Burnley, M. J.; Rubin, H. N.; Miera, J. A.; Reynolds, M. M. Porphyrin-Based Metal–Organic Framework and Polyvinylchloride Composites for Fluorescence Sensing of Divalent Cadmium Ions in Water. *Inorg. Chem. Commun.* **2020**, *115*, 107861.
- (67) Burger, T.; Winkler, C.; Dalfen, I.; Slugovc, C.; M. Borisov, S. Porphyrin Based Metal–Organic Frameworks: Highly Sensitive Materials for Optical Sensing of Oxygen in Gas Phase. *J. Mater. Chem. C* **2021**, *9*, 17099–17112.
- (68) So, M. C.; Jin, S.; Son, H. J.; Wiederrecht, G. P.; Farha, O. K.; Hupp, J. T. Layer-by-Layer Fabrication of Oriented Porous Thin Films Based on Porphyrin-Containing Metal–Organic Frameworks. *J. Am. Chem. Soc.* **2013**, *135*, 15698–15701.
- (69) So, M. C.; Beyzavi, M. H.; Sawhney, R.; Shekhah, O.; Eddaoudi, M.; Al-Juaid, S. S.; Hupp, J. T.; Farha, O. K. Post-Assembly Transformations of Porphyrin-Containing Metal–Organic Framework (MOF) Films Fabricated via Automated Layer-by-Layer Coordination. *Chem. Commun.* **2014**, *51*, 85–88.
- (70) Burnett, B. J.; Choe, W. Stepwise Pillar Insertion into Metal–Organic Frameworks: A Sequential Self-Assembly Approach. *CrystEngComm* **2012**, *14*, 6129–6131.
- (71) Goswami, S.; Ma, L.; Martinson, A. B. F.; Wasielewski, M. R.; Farha, O. K.; Hupp, J. T.

Toward Metal–Organic Framework-Based Solar Cells: Enhancing Directional Exciton Transport by Collapsing Three-Dimensional Film Structures. *ACS Appl. Mater. Interfaces* **2016**, *8*, 30863–30870.

(72) Braverman, M. A.; Nettleman, J. H.; Supkowski, R. M.; LaDuca, R. L. Copper Phthalate Coordination Polymers Incorporating Kinked Dipyridyl Ligands: An Unprecedented 8-Connected Network and One-Dimensional Chiral Nanobarrels with Hydrophobic Channels Constructed from Septuple Helical Motifs. *Inorg. Chem.* **2009**, *48*, 4918–4926.

(73) Liu, B.; Wei, L.; Li, N.; Wu, W.-P.; Miao, H.; Wang, Y.-Y.; Shi, Q.-Z. Solvent/Temperature and Dipyridyl Ligands Induced Diverse Coordination Polymers Based on 3-(2',5'-Dicarboxylphenyl)Pyridine. *Crys. Growth Des.* **2014**, *14*, 1110–1127.

(74) Dreischarf, A. C.; Lammert, M.; Stock, N.; Reinsch, H. Green Synthesis of Zr-CAU-28: Structure and Properties of the First Zr-MOF Based on 2,5-Furandicarboxylic Acid. *Inorg. Chem.* **2017**, *56*, 2270–2277.

(75) Joyce, J. T.; Laffir, F. R.; Silien, C. Layer-by-Layer Growth and Photocurrent Generation in Metal–Organic Coordination Films. *J. Phys. Chem. C* **2013**, *117*, 12502–12509.

(76) Franke, M.; Marchini, F.; Steinrück, H.-P.; Lytken, O.; Williams, F. J. Surface Porphyrins Metalate with Zn Ions from Solution. *J. Phys. Chem. Lett.* **2015**, *6*, 4845–4849.

(77) Yamashige, H.; Matsuo, S.; Kurisaki, T.; Perera, R. C. C.; Wakita, H. Local Structure of Nitrogen Atoms in a Porphine Ring of *Meso*-Phenyl Substituted Porphyrin with an Electron-

Withdrawing Group Using X-Ray Photoelectron Spectroscopy and X-Ray Absorption Spectroscopy.

Anal. Sci. **2005**, *21*, 635–639.

(78) Jakša, G.; Štefane, B.; Kovač, J. XPS and AFM Characterization of Aminosilanes with Different Numbers of Bonding Sites on a Silicon Wafer. *Surf. Interface Anal.* **2013**, *45*, 1709–1713.

(79) Graf, N.; Yegen, E.; Gross, T.; Lippitz, A.; Weigel, W.; Krakert, S.; Terfort, A.; Unger, W. E. S. XPS and NEXAFS Studies of Aliphatic and Aromatic Amine Species on Functionalized Surfaces. *Surf. Science* **2009**, *603*, 2849–2860.

(80) Choi, E.-Y.; Barron, P. M.; Novotny, R. W.; Son, H.-T.; Hu, C.; Choe, W. Pillared Porphyrin Homologous Series: Intergrowth in Metal–Organic Frameworks. *Inorg. Chem.* **2009**, *48*, 426–428.

Synopsis (75 words)

We report the effect of atmospheric water during layer-by-layer growth of MOF thin films on chemical composition, structure, and surface morphology. Coordination replacement of water with the organic linkers occurred more often at high RH, leading to imbalance in composition of two organic linkers of MOF thin film, contamination of the other phases than that observed at low RH, and rough surface. Our study demonstrates the importance of controlling humidity during MOF thin film fabrication.

